ACS OMEGA

http://pubs.acs.org/journal/acsodf

Article

Niobia Nanofiber-Reinforced Protective Niobium Oxide/Acrylate Nanocomposite Coatings

Ubong Eduok*

Cite This: *ACS Omega* 2020, 5, 30716−30728

Read Online

ACCESS | Metrics & More | Article Recommendations | Supporting Information

ABSTRACT: In the present study, the corrosion resistance of a new niobium oxide/acrylate hybrid nanocomposite coating doped with niobia nanofibers is investigated. Nanofibers were initially synthesized from niobium(V) chloride precursor in a novel autoclave approach before fabricating the base coating from a two-step process involving the syntheses of acrylate resin via free radical polymerization and niobium oxide gel from niobium ethoxide via a sol−gel technique. Variants of the synthesized nanocomposite coating were incorporated with varying concentrations of niobia nanofibers before spin-coating on Q235 steel substrates to inhibit corrosive electrolytic ion percolation and further enhance corrosion resistance when treated with chloride-enriched corrosive media. The corrosion resistance of these nanocomposite coatings increased with nanofiber content up to an optimum concentration due to the corrosion-inhibiting and protective effects of niobium barrier layers within these coatings. The presence of the niobia nanofibers also promoted improved surface contact angle and toughened mechanical strengths.

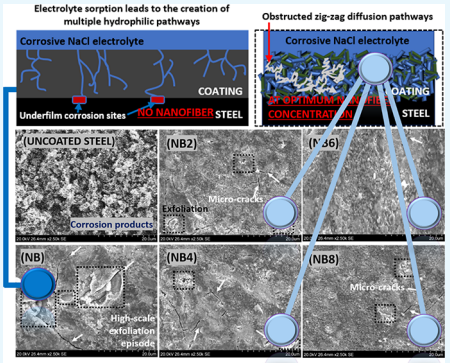

1. INTRODUCTION

Among the most effective approaches for inhibition or outright prevention of corrosion, the use of protective surface coatings has recorded significant successes, leading to several innovations in the field. Most of these protective coatings are designed to introduce surface-active oxide-forming components capable of forming stable secondary layers within the internal microstructures of the coatings.[1] Oxide-formers (e.g., Si, Ti, Cr, Al, Nb, etc.) have played unique roles in the syntheses of efficient protective coatings. They also played interesting roles in the fabrication of metallic materials with high thermal and stress resistance, deployed in aviation, pipeline, electronics, biomedicine, gas turbines, and defense applications.[2] The oxide-forming and IR thermal behavior of niobium metal and its protective coatings contribute to the understanding of its corrosion resistance, heat transfer, and transient thermal field characters.[2,3] The use of niobium compounds as complementary precursors to silane has shown promising trends in sol−gel chemistry for many material applications. The stabilities of niobium oxide, niobium/silicon composites, and niobium conversion coatings in corrosive substances and within some thermal conditions have also gained prominence in biomedical,[4,5] catalyst,[6,7] and protective magnesium engineering[8] applications. Most of these niobium materials are synthesized via sol−gel techniques due to their ease of applicability, low cost, and unique process chemistry.[3] However, their applicability may still completely rely on how they are synergistically used with other inorganic (Si, Zr, and Ti) components and in combination with some organic functionalities.[3] These organic−inorganic hybrid materials possess enhanced resistance against corrosion since they now possess combined properties of their organic (e.g., hydrophobicity) and inorganic oxide (e.g., chemical stability) components.[3]

Niobium may be very inert in nature. However, it also readily grows protective oxide layers (chemically identified as niobium pentoxide)[9−11] that contribute to enhanced corrosion resistance and biocompatibility.[12] Like most ceramic oxides (e.g., titania (TiO_2), silica (SiO_2), and zirconia (ZrO_2)) within coatings on metallic surfaces, niobia (Nb_2O_5) promotes surface adhesion and significant corrosion and wear resistances.[13] On coated metal surfaces, Nb_2O_5 becomes a coating additive capable of forming multifunctional anticorrosive barrier oxide films that further hinder the percolation of corrosive electrolytic ions toward the metal surface.[13] Although the presence of niobium barrier layers reduces electrolytic uptake, the protective performance of niobium-based coating composites eventually fails due to factors that may depend on (i) barrier protective effect of niobium, (ii) leaching of coating components via inherent microcracks, (iii) length of exposure of coatings to service environments, (iv) size of niobium nanofillers, etc.[14] These named causes of coating failure are some of the factors that contribute to the onset of corrosion on coated metal

Received: October 10, 2020
Accepted: November 5, 2020
Published: November 17, 2020

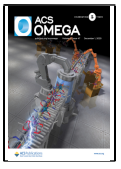

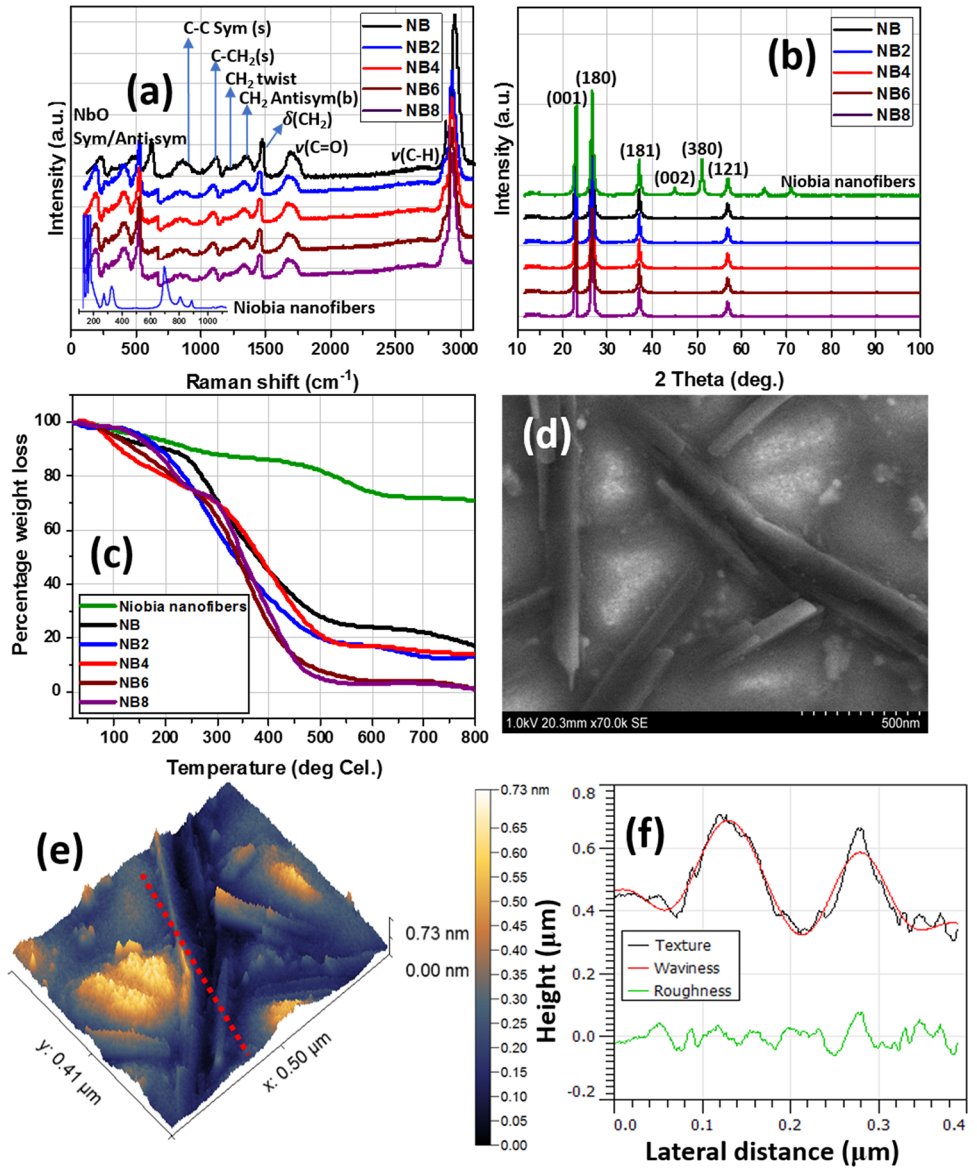

Figure 1. (a) Raman, (b) XRD, and (c) thermogravimetric spectra of niobia nanofibers and niobia-doped niobium oxide/acrylate nanocomposite coatings; (d) SEM and (e) AFM micrographs of niobia nanofibers; (f) corresponding surface profile showing changes in some surface parameters.

surfaces. However, failure mechanisms in niobium-based organic−inorganic hybrid coatings with niobium nanofillers are not clearly understood in neutral electrolytes. A number of researchers have investigated the corrosion resistance of niobium coatings on industrial steel metals in various service environments: strontium-incorporated Nb_2O_5 coating on stainless steel in simulated body fluid (SBF),[13] Ce-incorporated niobium oxide coated stainless steel in SBF,[14] niobium incorporated titanium oxide coating on stainless steel in SBF,[15] niobium carbide coatings produced on AISI 1045 steel in 3 wt % NaCl,[16] niobium coated 304 stainless steel in 0.7 M sulfuric acid,[17] to mention a few. Most of these examples are based on coating components with dissimilar chemistries. However, the incorporation of niobium barrier layers from a corrosion-inhibiting coating component (niobia nanofibers) with similar chemistry to those of the base coatings (niobium oxide/acrylate matrix) is proposed in this study.

In the present study, the use of niobia fillers within niobium oxide/acrylate hybrid material is proposed. Before incorporating them within the coating matrix, niobia nanofibers were synthesized from a niobium(V) chloride precursor by a novel autoclave approach. The niobium oxide/acrylate hybrid nanocomposite coating was synthesized from a two-step process involving the synthesis of acrylate resin via free radical polymerization and sol−gel preparation of niobium oxide from niobium ethoxide, slowly chelated with methacrylic acid at 50 °C. These nanofibers will serve as fillers needed to reinforce the internal microstructure of niobium oxide/acrylate nanocomposite coatings, increase their mechanical strengths, enhance their corrosion resistance, and encourage metal−surface coating adhesion. This work was also designed to determine the optimum concentration of nanofiber fillers required to prepare niobium oxide/acrylate hybrid nanocomposite coatings with efficient protective strengths against chloride-induced corrosion for industrial steel. Acrylate was the choice of organic acrylate resin component in this study due to its corrosion resistance in harsh conditions.[18] Acrylate resin coatings are susceptible to a decrease in protective strengths

https://dx.doi.org/10.1021/acsomega.0c04948
ACS Omega 2020, 5, 30716−30728

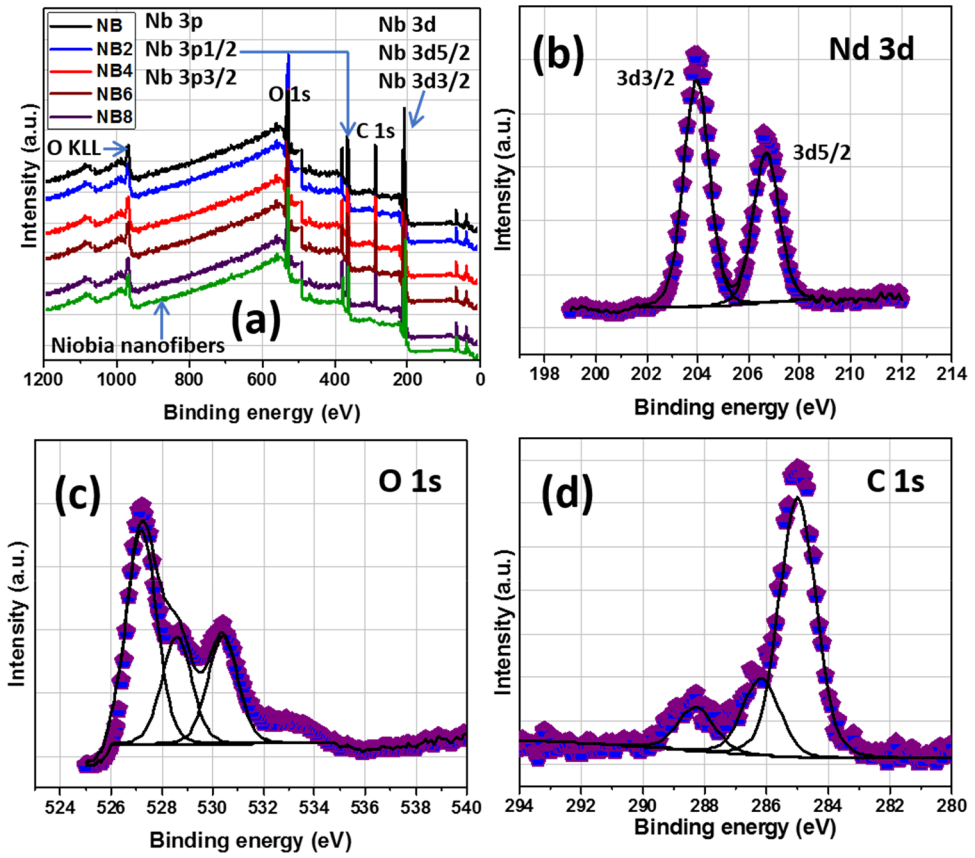

Figure 2. (a) Wide-scan and (b–d) high-resolution XPS spectra of niobia nanofibers and niobia-doped niobium oxide/acrylate nanocomposite coatings.

with time and may also degrade due to long-time environmental exposure,[18] and hence the need to incorporate niobia nanofillers. A mechanism for the barrier performance for this doped nanocomposite coating has also been proposed in order to best understand the relationship between corrosion resistance and coating content. There are several pieces of recent literature evidence on the use of inorganic pigments and coating fillers in acrylate resins: ZrO_2 nanoparticles,[18] graphene/CeO_2 nanoflakes,[19] SiO_2-Ag,[20] *h*-BN nanoflakes,[21] ZnO/graphene oxide,[22] SiO_2 nanoparticles,[23] Fe_3O_4-Ag,[24] MoS_2 nanosheets,[25] and carbon nanotubes,[26] to mention a few. Coatings with these inorganic fillers generally possess prolonged barrier performance due to the presence of these corrosion-inhibiting fillers incorporated to reinforce their internal microstructures.

2. RESULTS AND DISCUSSION

2.1. Characterization of Niobia Nanofibers and Niobia-Doped Nanocomposite Coatings. Before modifying the coating suspensions with the synthesized niobia (Nb_2O_5) nanofibers, both the Nb_2O_5 product and $NiCl_5$ precursor were characterized using appropriate techniques;[27,28] results are presented within the Supporting Information. Analyses with Raman spectroscopy revealed a D_{2h} symmetry consistent with pure powdery $NbCl_5$. The peaks at 374 and 394 cm^{-1} are attributed to its Nb−Cl stretching vibration and overlapping ν-1bands.[29,30] The solid-state spectrum of this inorganic Nb_2O_5 material is presented in Figure 1a, showing a distinct difference from the $NiCl_5$ precursor (Figure S1). The Raman peaks of the Nb_2O_5 nanofibers are not well-defined even after baseline correction, and this is indicative of poor crystallinity.[31] The intense peak at 717 cm^{-1} corresponds to symmetric and anti-symmetric stretching NbO vibration modes of Nb−O−Nb linkages.[27,32] Framework vibration bands related to oxygen are located between 500 and 1100 cm^{-1}.[31] The peaks of cations occupying octahedron and tetrahedron centers are located at 150−400 cm^{-1}. The presence of the Nb−O−Nb bending mode is responsible for the band at 235 cm^{-1}. Lu et al.[33] have also opined that Raman peaks around 800−900 cm^{-1} may be linked with symmetric stretch of Nb═O cm^{-1} are ascribed to bridging Nb−O−Nb vibrations. Most of these peaks are consistent with those expressed on the Raman spectra of the niobia-doped niobium oxide/acrylate nanocomposite coatings. The strong peaks at 2930 cm^{-1} represent C−H stretching vibration, while those at 1685 cm^{-1} could be linked with C═O carbonyl bonds.[34] Raman peaks from the C−C bond and CH_2 twisting signals could also be located around 1320 and 1120 cm^{-1}.[34,35] Vibration signals linked with C−COOH and C−CH_2 stretching are responsible for the peaks at 846 and 1086 cm^{-1}, respectively; other peaks are indicated on the spectra. The niobia nanostructure was also analyzed using XRD; corresponding spectra compared with those of niobia-doped niobium oxide/acrylate nanocomposite coatings are presented in Figure 1b. The diffraction patterns are consistent with a small crystal size and poor crystalline powdery Nb_2O_5 crystals. The X-ray adsorption peaks at (001), (180), (181), (002), (380), and (121) planes are due to Nb_2O_5 crystals.[36] These peaks are also present on the spectra of doped nanocomposite coating materials (NB2−NB8) and are also consistent with their crystalline interlayered network.

https://dx.doi.org/10.1021/acsomega.0c04948
ACS Omega 2020, 5, 30716−30728

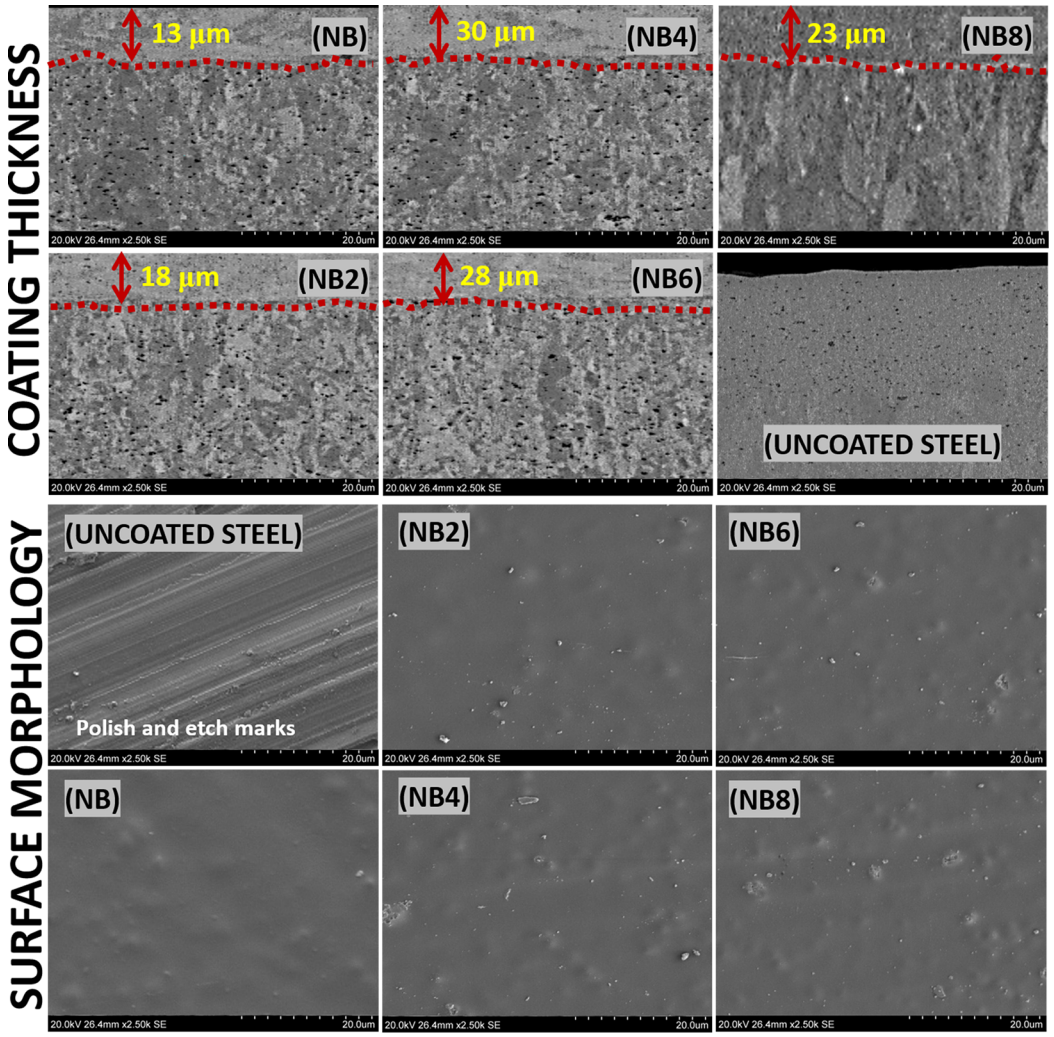

Figure 3. SEM micrographs showing mean coating thicknesses (X measured in μm) and surface morphologies of nanocomposite coating surfaces after spin coating.

The thermal behavior of these niobia nanofibers was also analyzed by means of thermogravimetric analysis (TGA); thermal curves are presented in Figure 1c. The evaporation of less strongly adsorbed water molecules from the crystalline nanostructure is responsible for the weight loss before 200 °C, while wider crystal transitions were observed beyond this temperature at a 10 °C/min heating rate. Reduced percentage of weight loss around 600 °C and beyond may be due to the transformation from hydrated N_2O_5 nanoparticles to more pseudohexagonal and orthorhombic crystalline particles.[37,38] There are also changes in thermal curves of the niobia-doped nanocomposite materials relative to those of the nanofibers. Also, the observed differences in TGA curves between these coating materials are due to variants in nanofiber content within the nanocomposite coatings as well as the inorganic/organic fragments of the coating network. This study also reveals the morphologies of the niobia N_2O_5 nanostructures synthesized from $NiCl_5$. The resultant niobia structures were nanofibers with nonuniform particles as presented in SEM micrographs in Figure 1d. The nanofiber morphology was also depicted by AFM (Figure 1e); their AFM image revealed nanostructures similar to those reflected in the SEM micrograph. These nanofibers have an average particle size of 105 nm and are unevenly dispersed and nonagglomerated together. Figure 1f displays changes in some surface properties profiled between heights and lateral distance between particles.

Apart from XRD, XPS analyses of niobia nanofibers and niobia-doped coatings were also conducted. The XPS wide-scan and high-resolution deconvoluted spectra are presented in Figure 2a. The latter spectra show core-level peaks consistent with the inorganic (Nb and O) and organic (C) components of the coatings; there is no C content in the XPS spectrum of the nanofiber. All high-resolution spectra were analyzed using Gaussian−Lorentzian combination from CasaXPS software. The Nd 3d spectrum (Figure 2b) shows dual peaks corresponding to 3d 3/2 (at 204 eV) and 3d 5/2 (at 207 eV) doublet spins consistent with Nb^{5+}.[38] Figure 3c,d also depicts XPS spectra with binding energies linked with O 1s and C 1s peaks. The high-intensity O 1s peaks at 529.6 eV could be assigned to O^{2-} in Nb oxide, while surface oxygen may be linked with the low-intensity peak at 531.9 eV.[38,39] The peak at 530.7 eV corresponds to residual C−O on the coating network,[38] while the C 1s XPS spectrum also shows peaks consistent with C═O and O−C═O bonds within the acrylate chain.[40] The nanoparticulate surface areas (S_{BET}) of the synthesized nanofiber are 51 and 45 m^2/g, and they were derived from BET analyses at calcination temperatures up to 500 and 600 °C,

https://dx.doi.org/10.1021/acsomega.0c04948
ACS Omega 2020, 5, 30716−30728

Table 1. Values of Aqueous Contact Angle (θ^{o}_{w}) and Vickers Hardness of Doped Niobium Oxide/Acrylate Nanocomposite Coatings on Steel Substrates[a]

		coated steel substrates				
types of tests conducted	uncoated steel	NB	NB2	NB4	NB6	NB8
aqueous contact angle (θ^{o}_{w})	30.0 ± 1.2	68.3 ± 1.4	68.2 ± 0.8	75.7 ± 1.0	90.5 ± 3.0	92.0 ± 3.0
	16.2 ± 1.1	34.5 ± 0.8	42.6 ± 0.6	54.8 ± 2.2	67.8 ± 0.5	62.2 ± 0.5
Vickers hardness (VH)	41.7 ± 0.4	52.8 ± 0.6	56.0 ± 1.3	59.3 ± 2.4	61.1 ± 0.2	63.8 ± 2.2

[a]The presented values of θ^{o}_{w} and VH are the mean of three repeated trial measurements; values of θ^{o}_{w} on the first and second rows were measured prior to and after corrosion test, respectively.

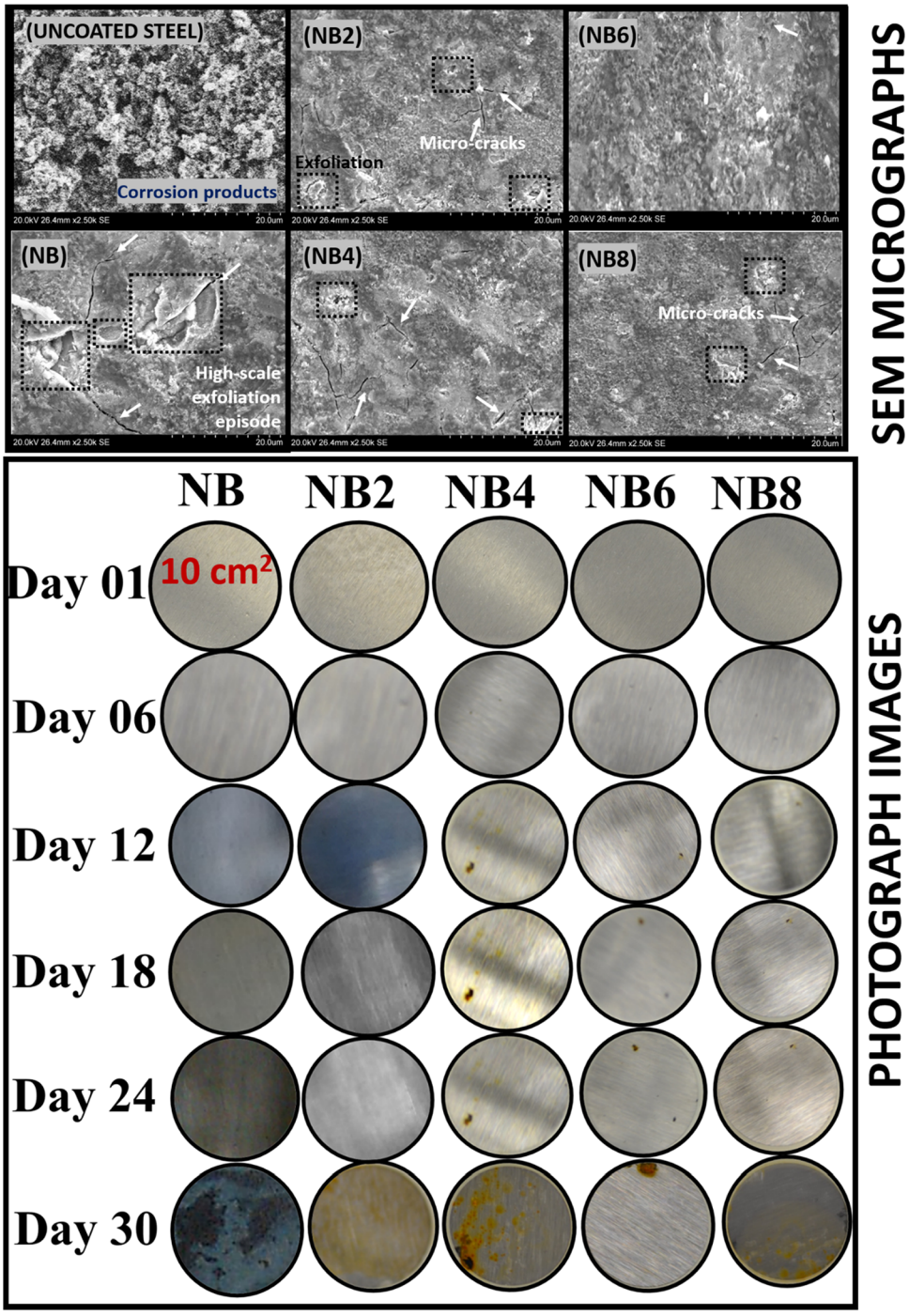

Figure 4. Surface appearances (SEM and photographs) of coated (NB, NB2−NB8) and uncoated steel surfaces after a month of continuous exposure to saline 3.5 wt % NaCl electrolytes.

https://dx.doi.org/10.1021/acsomega.0c04948
ACS Omega 2020, 5, 30716−30728

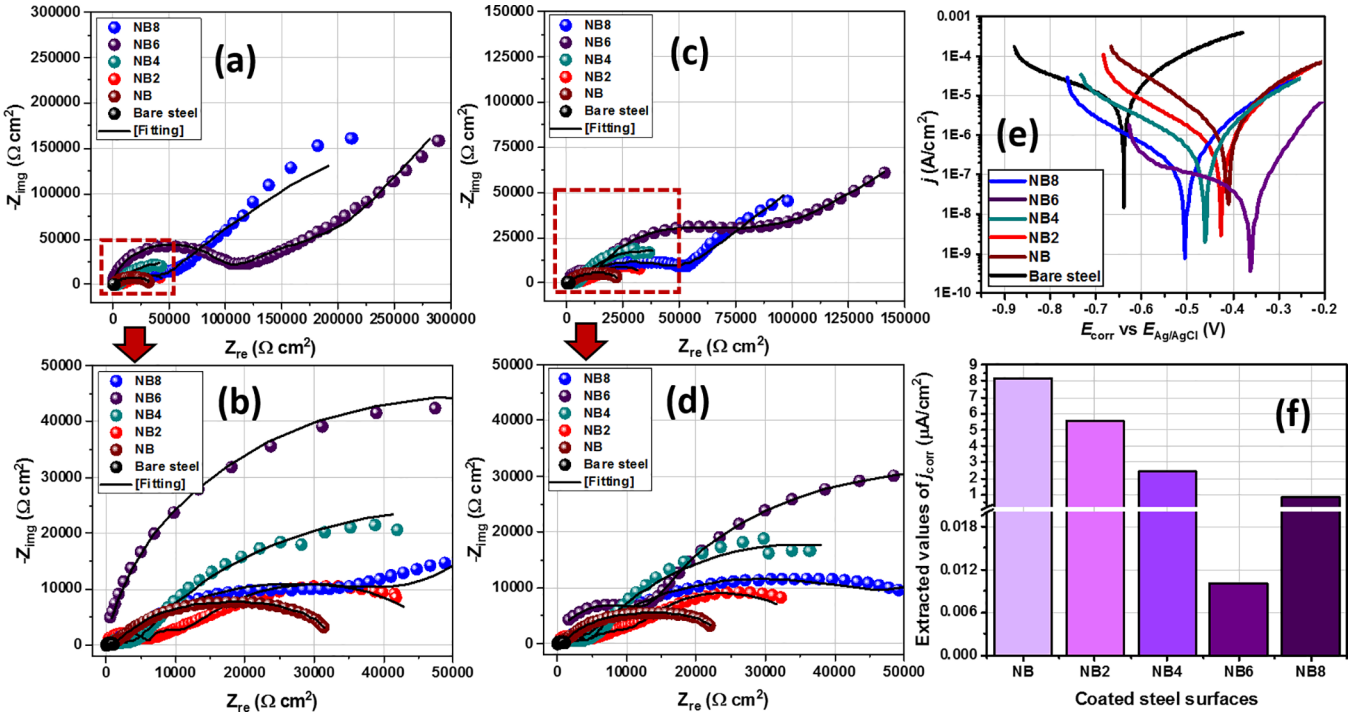

Figure 5. Nyquist curves for coated (NB, NB2−NB8) and uncoated steel substrates (a, b) immediately after immersion and (c, d) after 30 days of exposure in saline 3.5 wt % NaCl electrolytes; (e) potentiodynamic polarization curves were collected at the end of a month with (f) the corresponding values of j_{corr} derived from curves of respective substrates.

respectively. Values of S_{BET} for the niobia nanofibers were determined by means of the BET approach.[34]

2.2. Contact Angle and Microhardness of Nanocomposite Coatings. The mean aqueous contact angle (θ^{o}_{w}) of each coated surface was measured relative to the bare surface using the pendant drop approach; results are presented in Table 1. As expected, the magnitude of θ^{o}_{w} for the bare/uncoated surface stood at 30.0° due to adsorbed moisture while 68.3° was recorded for the undoped (NB) niobium oxide/acrylate coating. Values of (θ^{o}_{w}) were observed to increase in the order NB8 (92.0°) > NB6 (90.5°) > NB4 (75.7°) > NB0 (68.3°) > NB2 (68.2°); coated surfaces with lower niobia content were hydrophilic. However, this slowly changed for NB6 and NB8 with recorded hydrophobicity, and this could be attributed to the altered surface morphologies.[41,42] The degree of hydrophilicity increased, however, in all coated surfaces after chloride-induced treatment. The observed hydrophobic surfaces are direct contributions of the surface roughness due to the niobia nanoparticulates within the doped coatings. A similar trend was recorded for zirconia nanoparticles incorporated within acrylic coating on Q235 steel.[18,42] In order to probe the effect of niobia content on mechanical hardness, Vickers hardness values of respective coatings were measured and presented in Table 1. The mean values of microhardness of bare steel and the undoped coated (NB) substrates stood at 41.7 and 52.8 HV, respectively. However, the gross microhardness values increased with niobia concentrations; NB (52.8 HV) > NB2 (56.0 HV) > NB4 (59.3 HV) > NB6 (61.1 HV) > NB8 (63.8 HV). This could be attributed to matrix changes within the coatings once the particles were incorporated.[43] These niobia nanofibers reinforced the internal coating structures by increasing their bulk cross-linking density and mechanical strength.[44] Adding these nanoentities via bulk nanoparticulate dispersion during synthesis had also increased the microhardness of the nanocomposite coatings by grain refinement and dispersion strengthening.[45] The nanofibers also acted as inorganic fillers within the bulk of the nanocomposite coatings in such a way as to block hydrophilic transport channels of corrosive chloride molecules and ions chloride ions.[46] Compared to the undoped coatings, those encapsulated with nanofibers possessed prolonged bulk compactness and rigidity, less porosity, and elastic recovery.

2.3. Surface Morphological Analyses of Nanocomposite Coatings. Figure 3 depicts SEM micrographs showing coating thicknesses and surface morphologies of nanocomposite coatings after post spin-coating processes. The presented coating morphologies were revealed as an aftermath of the vacuum-cured procedure of coated niobia-reinforced nanocomposite suspensions on precleaned steel substrates. Each coating suspension was spun once in order to spread thin films at microscale mean thicknesses (X) as presented in Figure 3. Variants of these hybrid niobium oxide/acrylate nanocomposite coatings were fabricated from a two-step process involving the synthesis of acrylate resin via free radical polymerization and sol−gel preparation of niobium oxide from niobium ethoxide. The previously synthesized niobia nanofibers were then dispersed, and these agglomerated nanoparticles further roughened the amorphous gelled coating surfaces. The nanofibers were dispersed within the hybrid nanocomposite coating in order to enhance cross-linking densities between internal coating layers.[45,47] However, this did not significantly alter the coating thicknesses.

2.4. Effect of Chloride Treatment on Surface Morphologies of Nanocomposite Coatings. Inherent changes in surface morphology on each niobium oxide/acrylate nanocomposite coating were also examined after chloride treatment by means of electron microscopy. Figure 4 depicts observed microstructural defects on each nanocomposite coating after a

https://dx.doi.org/10.1021/acsomega.0c04948
ACS Omega 2020, 5, 30716−30728

month of consecutive exposure to the corrosive electrolyte. As represented in SEM and photograph images, the presence of the nanofibers infused within these nanocomposite coatings improved their gross rigidity. However, each surface appeared to be different after electrolyte adsorption due to their varying microlayer cross-linking densities. Compared to surfaces prior to the test, the impacted coating surfaces showed more exfoliation episodes in the forms of microcracks, pores, and disbonding on less protective barrier coatings. The adsorbed electrolyte with them further widened these defects by creating more hydrophilic transport channels while allowing migrating corrosive molecules toward the coating/metal interface. The undoped coating was almost completely disbonded due to continuous accumulation of the aqueous electrolyte beneath its film as a consequence of ionic migration.[47] However, these micropathways were further blocked within more corrosion-resistant coatings (i.e., with higher nanofiber contents, e.g., NB6 and NB8) since their internal coating networks were further strengthened, in turn, blocking these ionic routes.[46] The enhanced cross-linking densities and compactness of these doped coatings contributed to reduced gross bulk porosity and improved protective efficiency in the presence of these nanofibers. In this study, I observed reduced surface defects with nanofiber contents, from 0.2 to 0.6 mg (the latter being the optimum concentration in a 20 g coating suspension). However, the coating with 0.8 mg of nanofibers showed a significant presence of microcracks due to the broadening of narrow transverse channels by overpacked nanofibers within the already saturated coating matrix. This anomaly led to ionic migration through the widened pore channels toward the metal surface, in turn resulting in underfilm corrosion. The photograph images and those from SEM micrographs are consistent and in good agreement. Significant corrosion was observed on surface coatings with inferior protective performance after a month due to coating disbonding.

2.5. Measuring the Corrosion Resistance of Niobia-Doped Nanocomposite Coatings on Steel. In view of correlating the protective performances of nanocomposite coatings with nanofiber content, their corrosion resistances were measured by means of electrochemical techniques. Each test was conducted at 30 °C immediately after exposure to 3.5 wt % NaCl electrolyte and after 30 consecutive days. Nyquist curves for all coated working electrode substrates were recorded in a potentiostatic mode after applying 10 mV. These curves are presented in Figure 5a–d, and those with wider semicircle diameters are consistent with coating systems with superior impedance against steel corrosion and hence their enhanced corrosion resistance. A brief look reveals an increase in corrosion resistance with increasing niobia nanofiber content. Except for the impedance curve of the bare steel, others are two-time constant semicircles. These curves were fitted into equivalent circuit models in order to further explain the characteristic electrochemical behavior of respective nanocomposite coatings; extracted electrochemical parameters are presented in Table S1.

It is worth noting that the constant phase element (CPE, Q) was introduced in the circuit model as an alternate capacitor element to account for distortions within the electrical double layers rising from electrode surface irregularities. Its impedance is defined as $Z_{CPE} = [Y_o(j\omega)^{\alpha}]^{-1}$ where ω and j are the angular frequency and imaginary unit, respectively. α is the CPE's correlation coefficient whose values are within $0 < \alpha < 1$; it is also influenced by electrode surface roughness.[41,46,47] The first time constant at higher frequency, $R_{coating}$·$CPE_{coating}$, represents the direct behavior of the nanocomposite coating. $R_{coating}$ and $CPE_{coating}$ denote the pore resistance and CPE of the coating, respectively. $R_{coating}$ accounts for the opposition to the flow of corrosive ion currents through the coatings and also relates to coating porosity. Immediately after exposure to the electrolyte, its values increased with niobia nanoparticle content in the order NB6 (88.3 kΩ cm^2) > NB8 (54.5 kΩ cm^2) > NB4 (15.8 kΩ cm^2) > NB2 (10.2 kΩ cm^2) > NB (6.7 kΩ cm^2). However, lower values were recorded on day 30: 1.7, 2.5, 4.4, 30.4, and 20.1 kΩ cm^2, respectively. A closer look reveals that the niobium oxide/acrylate nanocomposite matrix with superior corrosion resistance was incorporated with 0.6 mg of niobia nanofibers (NB6). By far, it was the protective coating with the most compacted and highly cross-linked internal microstructure and hence inhibited corrosive flows through the coating.[46] The trend in the magnitude of $Q_{coating}$ was also probed. Lower values were recorded for NB6 for both durations, relative to other nanocomposite coatings, denoting that 0.6 mg was the optimum nanofiber concentration within the coatings, above which the corrosion resistance further dropped (in NB8). This could be attributed to conditions linked with supersaturation of the NB8 coating matrix with nanofibers. This must have led to the widened inherent transverse diffusion channels: a condition that further allowed for underfilm corrosion and subsequently coating disbonding due to high electrolyte uptake.[41,46,47] Higher values of $Q_{coating}$ were obtained for less protective coatings (i.e., at lower nanofiber content), and this was consistent with their loose internal structures, high rate of electrolyte adsorption, and water uptake within these coatings. Normally, dielectric constants of saline electrolytes are higher than those of host coatings.[48,49] Similar trends were also recorded for double layer capacitance (Q_{dl}) and charge transfer resistance (R_{ct}). Values of Q_{dl} on the second time constant represent the accumulation of ionic and water at the metal/coating interfaces. Magnitudes of $Q_{coating}$ for NB, NB2, NB4, NB6, and N8 were 125.5, 88.7, 28.8, 0.5, and 6.5 $\mu F\ cm^{-2}\ s^{-(1-\alpha c)}$ on the first day and 198.2, 156.9, 131.4, 51.5, and 99.1 $\mu F\ cm^{-2}\ s^{-(1-\alpha c)}$ on day 30 of exposure of coated substrates to 3.5 wt % NaCl. Like $Q_{coating}$, higher Q_{dl} values were obtained for all coatings at prolonged exposure duration and this is consistent with increased rate of electrolyte ion diffusion.[46,49] The charge transfer resistance (R_{ct}) followed the same trend as $R_{coating}$; its place within the second time constant at lower frequency represents the interphase close to the metal surface. This parameter represents the resistance of the metal/coating interface and rightly offers an idea about the onset of corrosion and coating disbonding from the steel surface. An impedance trend similar to results represented on the Nyquist curves is also depicted within the Bode phase angle curves for all doped niobium oxide/acrylate nanocomposite resin coatings (Figure S2).

Coating performance was also correlated with the magnitudes of corrosion current densities of respective coatings from the potentiodynamic polarization technique. This is a destructive electrochemical technique that induces corrosion on test substrates by applying potential in view of measuring their current densities as rates of electron exchange. The corresponding Tafel curves recorded from all coated steel substrates exposed to the saline corrodent are presented in Figure 5e. From these curves, values of corrosion current density (j_{corr}) and potential (E_{corr}) were derived and are presented in Figure 5f and Table S1. j_{corr} for all nanocomposite coatings significantly reduced with nanofiber content. The reinforced coatings impeded the flow of corrosive ion across the coating intended to induce localized corrosion upon reaching the metal surface.

https://dx.doi.org/10.1021/acsomega.0c04948
ACS Omega 2020, 5, 30716−30728

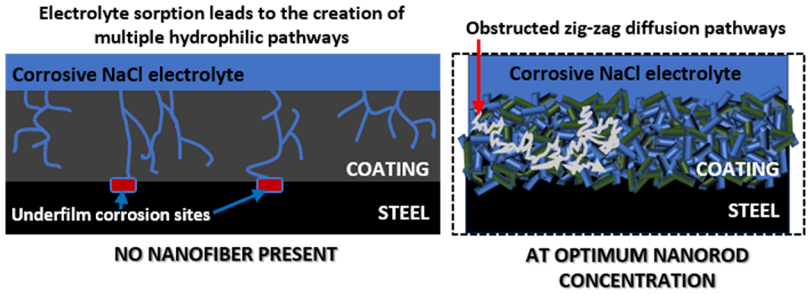

Figure 6. Mechanism of corrosion protection by niobia nanofibers. LHS: Without the nanofibers, the migration patterns toward the metal surface start with electrolyte sorption. Inherent microcracks within the coating network then allow for unhindered hydrophilic transport channels of corrosive molecules toward the metal surface, leading to the creation of wider cathodic corrosion sites.[41,46] RHS: The nanofibers further reinforced the internal microstructures of the niobium oxide/acrylate nanocomposite coating by creating mechanically interlocked, compact, and cross-linked coating networks. This subsequently retarded diffusion routes by blocking the permeating streams of corrosive electrolytes. Since the anticorrosive nanofibers also facilitate pore impermeability, diffusion pathways are zig-zag (i.e., in long meandering lines that curl and loop in irregular patterns), taking a significantly long time for the corrosive electrolyte to reach the metal surface; hence, corrosion is inhibited.[46,47]

Magnitudes of j_{corr} up to 8.2, 5.5, 2.4, 0.01, and 0.8 μA cm^{-2} were measured for NB, NB2, NB4, NB6, and NB8, respectively, relative to the bare steel substrate in NaCl (200.5 μA cm^{-2}). From this trend of results, it could be deduced that the niobium oxide/acrylate coating matrix encapsulated with 0.6 mg of niobia nanofibers had superior barrier performance.[46,47] Except for NB6 matrix, the extrapolated values of E_{corr} were also tending toward positive values with increasing concentrations. This trend denotes a mixed though predominantly anodic corrosion kinetics for coated steel substrates relative to the bare substrate. Since the applied potential aimed at inducing corrosion is also capable of damaging coating surfaces, Tafel experiments were conducted as the last test (after the EIS trials) at the end of day 30. The trend of results from both electrochemical techniques is consistent and is in agreement; corrosion resistance was largely enhanced in the presence of the nanofibers.

2.6. Mechanism of Enhanced Protective Performance by Niobia Nanofibers. Protective coatings with inherent secondary phases are reinforced when the nanofillers dispersed within them interlock between internal bonding networks, in turn, creating abrasion resistance and suppressed microcrack propagation.[50] Enforcement of the internal coating structures is designed to attain prolonged performance within their service environments since several factors may lead to minor blisters, mechanical abrasion, interfacial defects, surface disbonding, adhesion loss, and subsequently, surface coating failures.[51−53] Before failure, less protective coatings adsorb water molecules that further widens inherent micropores. In this study, the incorporation of niobia nanofibers within niobium oxide/acrylate nanocomposite coatings significantly increased their surface contact angle, toughened their mechanical strengths, and also promoted corrosion resistance. Corrosion resistance increased with nanofiber content up to an optimum concentration due to the corrosion-inhibiting and protective effects of niobium barrier layers within the internal microstructure of nanocomposite coatings. The extent of corrosion resistance of coatings was expressed in terms of inherent surface damage and induced pitting by means of scanning electron microscopy (Figure 4) and also by measuring coating resistances (Figure 5) using electrochemical techniques. The mechanism of corrosion protection by niobia nanofibers is presented in Figure 6. At optimum nanofiber concentration (0.6 mg in 20-g coating suspension), corrosion resistance was enhanced, and this was consistent with less electrolytic uptake and delayed underfilm steel corrosion since there were limited surface microcracks and pores on the coating surface (NB6). These nanofibers must have further reinforced the internal microstructure of the niobium oxide/acrylate nanocomposite coating by creating mechanically interlocked, compact, and cross-linked coating network. This contributed to retarding diffusion routes by blocking the permeating streams of corrosive electrolytes as pore permeability was reduced. The presence of these nanofibers must have altered the corrosive electrolyte diffusion pathways to meandering irregular patterns, thereby taking a significantly long time for them to reach the metal surface and hence inhibits corrosion.[53,54]

As presented in the LHS, without the nanofibers (i.e., for NB coating), the migration patterns toward the metal after electrolyte sorption are unrestricted. Inherent microcracks within this loosely structured coating allow for unaltered hydrophilic diffusion pathways, leading to creation of several cathodic sites and subsequently underfilm corrosion. The presented scheme (in Figure 6) is consistent with the Nguyen model for ionic transport channels in degraded/ageing coatings.[46,47] Less electrolytic uptake was observed in the presence of these nanofibers. This was attributed to the creation of more barrier layers within the doped nanocomposite coatings with an increment in niobium concentration. Niobium oxide/acrylate nanocomposite coatings with superior corrosion resistance possess cross-linked internal structures and also reduced bulk volume.[53] Like other reinforced fillers on coated steel surfaces, Nb_2O_5 nanofibers became unique coating additives capable of forming multifunctional anticorrosive barrier oxide films that further hindered the percolation of corrosive electrolytic ions toward the metal surface.[55−59] Comparative barrier performances of different coatings incorporated with niobia nanoparticles within this study and in those reported in the literature are presented in Table 2.

3. CONCLUSIONS

The following conclusions were drawn from experimental results obtained within this study:

1. Niobia nanofibers were synthesized from a niobium(V) chloride precursor in an autoclave approach, while the base coating was fabricated from a two-step process involving the syntheses of acrylate resin via free radical polymerization and niobium oxide gel from niobium ethoxide via a sol−gel technique.

https://dx.doi.org/10.1021/acsomega.0c04948
ACS Omega 2020, 5, 30716−30728

Table 2. Comparative Barrier Performances of Different Coatings Incorporated with Niobia Nanoparticles within This Study and in the Literature

S/No	coating type/metallic substrate/corrodent	niobium-based additives	coating technique	major findings/remarks about barrier performance	ref
1	niobium oxide/acrylate hybrid nanocomposite coating/Q235 steel/3.5 wt % NaCl	niobia nanofibers	spin coating	Niobia (Nb_2O_5) nanofibers enhanced the protective performance of the acrylate nanocomposite coatings by blocking inherent transverse channels against percolating corrosive ions, thus, inhibiting underfilm steel corrosion. The presence of niobia nanofibers enhanced the surface contact angle of the coatings while also toughening their mechanical strengths.	this study
2	Sr-doped niobia coating/316 stainless steel/simulated body fluid	none. Only niobia base coating with Sr additives	spin coating	The coating developed a self-healing effect due to the presence of Sr additives. However, its bioactivity and corrosion resistance depended on its morphology and Sr release rate.	[13]
3	Ce-incorporated niobia coating/316 stainless steel/simulated body fluid	none. niobia base coating with Ce additives	dip coating	Ce-doped niobia coating retained its nanostructure, morphology, and hydrophilicity. This contributed to an efficient self-healing behavior on stainless steel due to formation of protective oxide layers within the base coatings.	[14]
4	niobia-doped TiO_2 coating/316L stainless steel/simulated body fluid	niobia nanoparticles	spin coating	The presence of niobia within the TiO_2 coating led to the formation of a crystalline phase and barrier layers, leading to a reinforced nanostructure, increased hydrophobicity, and coating hardness as well as promoted metal−surface adhesion. Corrosion resistance was enhanced by formation of barrier layers within the coating; this also prevented the ingression of corrosive ions within the coating.	[15]
5	niobium carbide coating/AISI 1045 low alloy steel/3 wt % NaCl	none. only niobium carbide base coating; no additives involved	Thermoreactive deposition/diffusion technique	The corrosion resistance of carbide coatings increased with inherent niobium oxide phases. However, this parameter decreased after 24 h within the saline corrodent due to the creation of pores within the coatings.	[16]
6	organosilicon coating/low carbon steel/3.5 wt % NaCl	niobia additive	surface coating application using brush	Corrosion resistance of organosilicon coating was enhanced in the presence of Nb_2O_5 additives. This was attributed to the formation of cross-linking bonds between reinforced coating layers induced by niobia particles.	[60]
7	Niobia Nb_2O_5 and $(Nb_yCu_{1-y})O_x$ coating/Ti6Al4V titanium alloy/0.5 M NaCl, 2 g/L KF (pH = 2)	niobia and copper nanoadditives	magnetron sputtering technique	The presence of Cu additives within the niobia coatings enhanced its gross hardness and corrosion resistance, leading to decreased corrosion current density and shifts in corrosion potentials.	[61]
8	niobia coatings/Ti6Al4V titanium/simulated body fluid	niobia nanoparticles	electron beam deposition	Coating matrix electron beam deposited and annealed at 800 °C developed more stable Nb_2O_5 secondary nanocrystalline phases that contributed to enhanced hydrophobicity, reduced porosity, and enhanced corrosion resistance.	[62]

https://dx.doi.org/10.1021/acsomega.0c04948
ACS Omega 2020, 5, 30716−30728

2. Variants of this synthesized nanocomposite coating were made by incorporating varying concentrations of niobia nanofibers and then spin-coated on Q235 steel substrates. The corrosion resistance of these nanocomposite coatings increased with nanofiber content up to an optimum concentration due to the corrosion-inhibiting and protective effects of niobium barrier layers within the internal microstructure of these coatings.
3. Beyond the optimum nanofiber content (0.8 mg; i.e., for NB8), the coating resistance reduced due to oversaturation of the internal coating network with nanofibers; this trend was observed for both exposure durations under study. Values of $R_{coating}$ up to 88.3 and 54.5 kΩ cm^2 were recorded for NB6 (0.6 mg) and NB8 (0.8 mg), respectively, immediately after exposure of coated substrates to the corrodent and 30.4 and 20.1 kΩ cm^2 after 30 days.
4. Protective performance was expressed in terms of inherent surface damage and chloride-induced pitting by means of scanning electron microscopy and also by measuring coating resistances using electrochemical techniques.
5. This study proposes the incorporation of niobium barrier layers from a corrosion-inhibiting coating component with similar chemistry to those of the base coatings.
6. The presence of the niobia nanofibers was observed to also increase the surface contact angle of the nanocomposite coatings while also toughening their mechanical strengths.

4. EXPERIMENTAL PROCEDURES

4.1. Reagents and Materials. Niobium(V) chloride ($NiCl_5$, 99% purity) was the inorganic precursor for synthesizing the niobia nanofibers; it was purchased from Sigma Aldrich. Ethylene glycol methacrylate (99%), methacrylic acid (99%), acrylic acid (≥99%), methyl methacrylate (99%), and *tert*-butyl acrylate (98%) were utilized as precursors for acrylate resins. They were also purchased from Sigma Aldrich. The azobisisobutyronitrile free radical initiator (AIBN, 98%) in styrene (45%), ethanol (99%), niobium ethoxide (99.95%, NbOEt), and nitric acid (70%, HNO_3) were purchased from Sigma Aldrich and Merck Chemical Co, respectively. Purchased reagents containing concentrations of monomethyl ether hydroquinone (MEHQ) inhibitor were removed using prepacked columns as inhibitor removers. Deionized water was used for preparing all regents; it also had an 18.2 MΩ resistivity. All reagents and chemicals were purchased as analytical-grade reagents and used without further purification. All coatings were applied on Q235 steel grade working substrates in this study. Smaller masses from this steel grade were cut into 15 cm × 15 cm × 0.3 cm coupons, abraded with the aid of 400−4000 grit silicon carbide paper before a 30 s 5% Nital etching in order to promote metal−surface coating adhesion. Each steel substrate was degreased with ethanol and precleaned in accordance with the ASTM D609 standard. The chemical composition of the Q235 steel substrate is presented in Table 3.

Table 3. Chemical Composition of Q235 Steel Grade Utilized in this Study (the Balance Is Fe)

composition	C	Mn	Si	S	P
wt %	0.14−0.22	0.30−0.65	0.30	≤0.050	0.045

4.2. Synthesis of Niobia Nanofibers. Niobia (Nb_2O_5) nanofibers were synthesized using a yellow crystalline $NbCl_5$ precursor from a procedure previously reported in ref 27 with modification. From a stock of a $NbCl_5$ powdery sample oxidized overnight in the open, about 0.20 g was dispersed in 30 mL of deionized water (18.2 MΩ) and 30 mL of ethanol in a 2 h prehydrolysis stir at 30 °C. This was closely followed by an hour of sonication of the powder suspension before transferring into a Teflon-lined autoclave (100 mL) and placed in a pre-heated oven at 220 °C for 120 h. The autoclaved sample was allowed to cool at room temperature, centrifuged (15,000 rpm; Sorvall X4 Centrifuge, ThermoFisher) in ethanol, and then washed with ethanol and subsequently water repeatedly before 24 h of drying in an oven at 100 °C for 48 h. The resultant off-white Nb_2O_5 particles from this technique were not uniform, so they were further sieved to obtain finer nanoparticles and the rest were ball-milled.

4.3. Synthesis of Niobia Reinforced Hybrid Niobium Oxide/Acrylate Nanocomposite Coatings. A detailed schematic showing the synthesis of niobium oxide/acrylate hybrid nanocomposite coatings is presented in Figure 7. The first step of the coating process involved the synthesis of acrylate resin by free radical polymerization using a combination of acrylate precursors: 2 g of ethylene glycol methacrylate, methacrylic acid, and acrylic acid 3 g of methyl methacrylate and *tert*-butyl acrylate. This reaction was carried out in a 250 mL three-neck round-bottom flask (side necks bevelled, angle of 20°) coupled with a mechanical stirrer and a thermometer. The reaction was allowed to continue by continuous stirring (1500 rpm) at 70 °C for 2 h in the presence of AIBN (0.1 g) and styrene (1 g) before 30 min of sonication. While a second reaction was conducted simultaneously, a significant discoloration and increase in acrylate resin suspension viscosity was also observed. In a second flask, NbOEt was chelated with methacrylic acid at equimolar concentrations for an hour, after NbOEt was prehydrolyzed in 0.01 M HNO_3 catalyst using 1:1 ethanolic water as a diluent for 30 min at 50 °C. The final molar ratio of the chemicals was placed at 2.5:2.5:2:2:0.2 for methacrylic acid, NbOEt, EtOH/H_2O, and HNO_3, respectively. Solutions from each flask (amounting to 50 mL each) were then blended by stirring for 24 h at 750 rpm at 50 °C. The resultant solution was warm, signifying some form of exothermic reaction; it was also hazy in the first hour and later became completely clear with a colloidal feel, suggestive of a chemical reaction and not a physical dispersion. About 0.2 mg of synthesized niobia nanofibers was added to 20 g of as-synthesized nanocomposite coating suspension before the end of the second hour. This was conducted under an inert atmosphere in order to reinforce its internal microstructure during room-temperature curing for 24 h. This hybrid coating suspension itself was stable at room temperature for over a week.

4.4. Spin-Coating and Curing Procedures. The coating procedure utilized in this study was the spin coating from a Laurell Tech spin coater; a procedure utilized in depositing uniform thin coatings on flat precleaned steel surfaces. Less than 5 mL of coating suspension was used per coating type while spinning each metallic steel substrates (10 cm^2) at 10,000 rpm to spread thin films at microscale thicknesses via centrifugal force. The prepared niobia-reinforced hybrid niobium oxide/acrylate nanocomposite suspension was further vacuum-cured (at 50 °C for 24 h at 5 °C/min) before room-temperature curing and then labeled according to the weights of nanofibers. The steel substrates coated with nanocomposite suspension with 0.2, 0.4,

https://dx.doi.org/10.1021/acsomega.0c04948
ACS Omega 2020, 5, 30716−30728

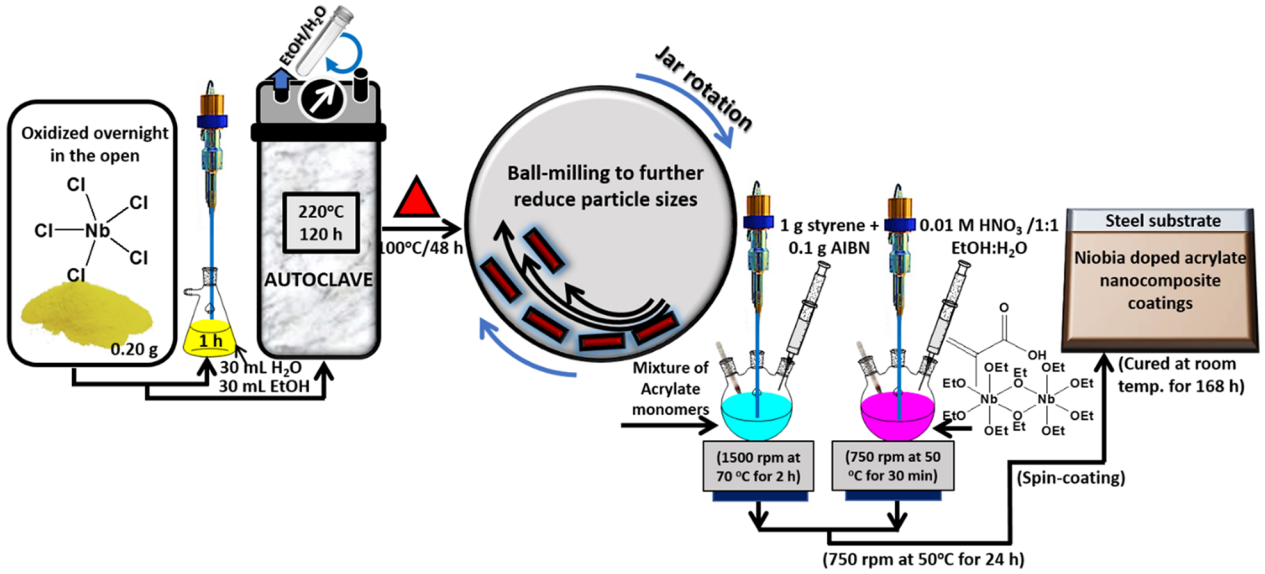

Figure 7. Annotated schematic depiction of the synthesis protocol for niobia nanofibers and niobia-doped niobium oxide/acrylate nanocomposite coating on steel.

0.6, 0.8 and 0 mg of nanofibers were labeled NB2, NB4, NB6, NB8, and NB, respectively.

4.5. Characterization of Niobia Nanofibers and Niobia-Reinforced Nanocomposite Coatings. Characterization of niobia nanofibers and niobia-reinforced nanocomposite coatings was carried out using different techniques. Raman measurements were conducted using a Renishaw Raman InVia reflex microscope (Renishaw, UK) from a 514 nm edge laser using extended grating. The crystallographic characterizations of these coating materials were also carried out by means of X-ray diffraction (Bruker D8 Discover XRD Diffractometer) at 40 mA and 40 kV with Cu Kα radiation. All scans were made with 2θ ranging between 10 and 100° at a 0.02° step size. The chemical compositions of these niobia nanofibers and niobia-reinforced nanocomposite coatings were also determined using an X-ray photoelectron spectroscopy XPS Kratos AXIS Supra system equipped with a 500 mm Rowland circle monochromated Al Kα (1486.6 eV) source and combined hemispherical and spherical-mirror analyzers. Thermogravimetric analysis (TGA) experiments were conducted from 5 mg of samples of both materials using a TGA SDT Q600 analyzer after placing them in Pt crucibles. Weight loss−temperature curves of these samples were recorded and analyzed from appropriate software from the instrument after analyses in a mixed N_2/O_2 atmosphere (both placed at 50 mL/min flow rate) at 5−20 °C/min heating rates. Inherent oxidative volatile products from the test were eliminated from the first N_2 flow rate.[28] In order to investigate changes in surface morphology between both materials after synthesis and metal−surface coating, these materials were viewed under a scanning electron microscope with the aid of a Hitachi SU6600 SEM. The microstrengths tests of coated surfaces were carried out using a Dynamic microhardness tester (Micro-Combi, CSM Instruments) equipped with a Vickers pyramid indenter. A maximum of 100 gf load was applied with a dwell duration of 15 s. In order to determine the hydrophobicity of each coating surfaces, their aqueous contact angles (θ_w^o) were investigated using a DataPhysics Instrument. After measurements, the values of θ_w^o for each surface were extrapolated after surface analyses by a pendant drop method. The surface area (S_{BET}) of the niobia nanofibers was analyzed using a Micromeritics Accelerated SA instrument at 0.10−0.15 relative pressure using the Brunauer−Emmett−Teller (BET) approach. The stored powder was initially degassed for an hour at 120 °C before raising the calcination temperature to the desired range.

4.6. Measuring Corrosion Impact on Coatings. Electrochemical techniques were utilized to study the corrosion resistance of these new niobium oxide/acrylate hybrid nanocomposite coatings in view of understanding their protective performances. These were accomplished by monitoring the electrochemical behaviors of completely immersed coated steel substrates exposed to aerated 3.5 wt % NaCl at 30 °C. These tests were conducted using a three-electrode cell system composed of a platinum auxiliary electrode and a Ag/AgCl (sat. KCl) reference electrode (in a Luggin capillary) connected to potentiostat/galvanostat/ZRA (Interface 1000, Gamry Instruments). The coated steel substrates were utilized as working electrodes.[28] EIS measurements were measured at open circuit potential (OCP) with respect to the reference electrode within a 0.01 to 100000 Hz frequency range. EIS spectra were recorded after applying an AC signal of 10 mV (rms) using the single sine technique. An equivalent circuit simulation program with EChem Analyst was utilized for all data analyses, creating equivalent circuit models and fitting experimental data. Before the theoretical data fitting to circuit models, the linearity of impedance spectra was determined using Kramers−Kronig transformation. Tafel polarization experiments were conducted by applying from −0.5 up to 0.5 V versus (Ag/AgCl (sat. KCl)) at a sweep rate of 0.5 mV/s. Both anodic and cathodic polarization measurements were conducted in the same experimental run.[28] The impact of chloride ion corrosion on the surface morphologies of these coated steel substrates was also investigated after a month of exposure to saline electrolyte using a scanning electron microscope. Surface changes after corrosion on each coating were compared to the appearances prior to the corrosion test; inherent differences were considered as the extent of protective performances of coatings (NB2−NB8) relative to uncoated steel (NB) substrates.

https://dx.doi.org/10.1021/acsomega.0c04948
ACS Omega 2020, 5, 30716−30728

■ ASSOCIATED CONTENT

Supporting Information

The Supporting Information is available free of charge at https://pubs.acs.org/doi/10.1021/acsomega.0c04948.

Raman, XPS, XRD, TGA spectra of niobia nanofibers and niobium chloride precursor; SEM and AFM micrographs of niobia nanofibers and niobium chloride precursor (Figure S1); electrochemical parameters for bare and doped nanocomposite coated steel substrates in 3.5 wt % NaCl (Table S1); Bode phase−angle curves for coated and uncoated steel substrates immediately after immersion and after 30 days of exposure to saline 3.5 wt % NaCl electrolytes (Figure S2) (PDF)

■ AUTHOR INFORMATION

Corresponding Author

Ubong Eduok − *College of Engineering, University of Saskatchewan, Saskatoon, Saskatchewan S7N 5A9, Canada;* orcid.org/0000-0002-4476-4841; Phone: +1 (306) 966 7752; Email: ubong.eduok@usask.ca; Fax: +1 (306) 966 5427

Complete contact information is available at: https://pubs.acs.org/10.1021/acsomega.0c04948

Notes

The author declares no competing financial interest.

■ ACKNOWLEDGMENTS

The author wishes to acknowledge the University of Saskatchewan for providing the facilities for this study. This experimental work was initiated and completed while the author was still at the Department of Mechanical Engineering, University of Saskatchewan, Saskatchewan, Canada.

■ REFERENCES

(1) Melo, D.; Sigüenza, D.; Salas, O.; Oseguera, J.; Reichelt, R.; López, V. M. Production, characterization and evaluation of protective Cr oxide coatings against metal dusting. *Surf. Coat. Technol.* **2009**, *204*, 788−792.

(2) Ge, Y. L.; Wang, Y. M.; Zhang, Y. F.; Guo, L. X.; Jia, D. C.; Ouyang, J. H.; Zhou, Y. The improved thermal radiation property of SiC doped microarc oxidation ceramic coating formed on niobium metal for metal thermal protective system. *Surf. Coat. Technol.* **2017**, *309*, 880−886.

(3) Varma, P. C. R.; Periyat, P.; Oubaha, M.; McDonagh, C.; Duffy, B. Application of niobium enriched ormosils as thermally stable coatings for aerospace aluminium alloys. *Surf. Coat. Technol.* **2011**, *205*, 3992−3998.

(4) Velten, D.; Eisenbarth, E.; Schanne, N.; Breme, J. Biocompatible Nb_2O_5 thin films prepared by means of the sol−gel process. *J. Mater. Sci.: Mater. Med.* **2004**, *15*, 457−461.

(5) Rosatto, S. S.; Sotomayor, P. T.; Kubota, L. T.; Gushikem, Y. SiO_2/Nb_2O_5 sol−gel as a support for HRP immobilization in biosensor preparation for phenol detection. *Electrochim. Acta* **2002**, *47*, 4451−4458.

(6) Aronne, A.; Marenna, E.; Califano, V.; Fanelli, E.; Pernice, P.; Trifuoggi, M.; Vergara, A. Sol−gel synthesis and structural characterization of niobium-silicon mixed-oxide nanocomposites. *J. Sol-Gel Sci. Technol.* **2007**, *43*, 193−204.

(7) Francisco, M. S. P.; Landers, R.; Gushikem, Y. Local order structure and surface acidity properties of a Nb2O5/SiO2 mixed oxide prepared by the sol−gel processing method. *J. Solid State Chem.* **2004**, *177*, 2432−2439.

(8) Marcus, P., Ardelean, H. Patent PCT/FR 02/01843. WO 02/097164 A2, 2002, US Patent 2007, 7, 156 905.

(9) Stojadinović, S.; Tadić, N.; Radić, N.; Stefanov, P.; Grbić, B.; Vasilić, R. Anodic luminescence, structural, photoluminescent, and photocatalytic properties of anodic oxide films grown on niobium in phosphoric acid. *Appl. Surf. Sci.* **2015**, *355*, 912−920.

(10) Pereira, B. L.; Lepienski, C. M.; Mazzaro, I.; Kuromoto, N. K. Apatite grown in niobium by two-step plasma electrolytic oxidation. *Mater. Sci. Eng., C* **2017**, *77*, 1235−1241.

(11) Sowa, M.; Kazek-Kęsik, A.; Krząkała, A.; Socha, R. P.; Dercz, G.; Michalska, J.; Simka, W. Modification of niobium surfaces using plasma electrolytic oxidation in silicate solutions. *J. Solid State Electrochem.* **2014**, *18*, 3129−3142.

(12) Quintero, D.; Gómez, M. A.; Araujo, W. S.; Echeverría, F.; Calderón, J. A. Influence of the electrical parameters of the anodizing PEO process on wear and corrosion resistance of niobium. *Surf. Coat. Technol.* **2019**, *380*, 125067.

(13) Pauline, S. A.; Rajendran, N. Effect of Sr on the bioactivity and corrosion resistance of nanoporous niobium oxide coating for orthopaedic applications. *Mater. Sci. Eng., C.* **2014**, *36*, 194−205.

(14) Katta, P. P.; Nalliyan, R. Corrosion resistance with self-healing behavior and biocompatibility of Ce incorporated niobium oxide coated 316L SS for orthopedic applications. *Surf. Coat. Technol.* **2019**, *375*, 715−726.

(15) Pauline, S. A.; Rajendran, N. Corrosion behaviour and biocompatibility of nanoporous niobium incorporated titanium oxide coating for orthopaedic applications. *Ceram. Int.* **2017**, *43*, 1731−1739.

(16) OrjuelaG, A.; Rincón, R.; Olaya, J. J. Corrosion resistance of niobium carbide coatings produced on AISI 1045 steel via thermo-reactive diffusion deposition. *Surf. Coat. Technol.* **2014**, *259*, 667−675.

(17) Pan, T. J.; Chen, Y.; Zhang, B.; Hu, J.; Li, C. Corrosion behavior of niobium coated 304 stainless steel in acid solution. *Appl. Surf. Sci.* **2016**, *369*, 320−325.

(18) Eduok, U.; Szpunar, J.; Ebenso, E. Synthesis and characterization of anticorrosion zirconia/acrylic nanocomposite resin coatings for steel. *Prog. Org. Coat.* **2019**, *137*, 105337.

(19) Li, H.; Wang, J.; Yang, J.; Zhang, J.; Ding, H. Large CeO_2 nanoflakes modified by graphene as barriers in waterborne acrylic coatings and the improved anticorrosion performance. *Prog. Org. Coat.* **2020**, *143*, 105607.

(20) Le, T. T.; Nguyen, T. V.; Nguyen, T. A.; Nguyen, T. T. H.; Thai, H.; Tran, D. L.; Dinh, D. A.; Nguyen, T. M.; Lu, L. T. Thermal, mechanical and antibacterial properties of water-based acrylic Polymer/SiO_2−Ag nanocomposite coating. *Mater. Chem. Phys.* **2019**, *232*, 362−366.

(21) Zou, B.; Chang, X.; Yang, J.; Wang, S.; Xu, J.; Wang, S.; Samukawa, S.; Wang, L. Plasma treated h-BN nanoflakes as barriers to enhance anticorrosion of acrylic coating on steel. *Prog. Org. Coat.* **2019**, *133*, 139−144.

(22) Sharifalhoseini, Z.; Entezari, M. H.; Davoodi, A.; Shahidi, M. Surface modification of mild steel before acrylic resin coating by hybrid ZnO/GO nanostructures to improve the corrosion protection. *J. Ind. Eng. Chem.* **2020**, *83*, 333−342.

(23) Bui, T. M. A.; Nguyen, T. V.; Nguyen, T. M.; Hoang, T. H.; Nguyen, T. T. H.; Lai, T. H.; Tran, T. N.; Nguyen, V. H.; Hoang, V. H.; Le, T. L.; Tran, D. L.; Dang, T. C.; Vu, Q. T.; Nguyen-Tri, P. Investigation of crosslinking, mechanical properties and weathering stability of acrylic polyurethane coating reinforced by SiO_2 nanoparticles issued from rice husk ash. *Mater. Chem. Phys.* **2020**, *241*, 122445.

(24) Nguyen, T. N. L.; Do, T. V.; Nguyen, T. V.; Dao, P. H.; Trinh, V. T.; Mac, V. P.; Nguyen, A. H.; Dinh, D. A.; Nguyen, T. A.; Vo, T. K. A.; Tran, D. L.; Le, T. L. Antimicrobial activity of acrylic polyurethane/Fe_3O_4-Ag nanocomposite coating. *Prog. Org. Coat.* **2019**, *132*, 15−20.

(25) Gao, F.; Du, A.; Ma, R.; Lv, C.; Yang, H.; Fan, Y.; Zhao, X.; Wu, J.; Cao, X. Improved corrosion resistance of acrylic coatings prepared with modified MoS_2 nanosheets. *Colloids Surf., A* **2020**, *587*, 124318.

(26) Song, D.; Yin, Z.; Liu, F.; Wan, H.; Gao, J.; Zhang, D.; Li, X. Effect of carbon nanotubes on the corrosion resistance of water-borne acrylic coatings. *Prog. Org. Coat.* **2017**, *110*, 182−186.

(27) Ullah, H.; Guerin, K.; Bonnet, P. Synthesis of Nb_2O_5 Nanoplates and their Conversion into NbO_2F Nanoparticles by Controlled Fluorination with Molecular Fluorine. *Eur. J. Inorg. Chem.* **2019**, *2019*, 230−236.
(28) Eduok, U.; Ohaeri, E.; Szpunar, J.; Akpan, I. Synthesis, characterization and application of glucosyloxyethyl acrylate graft chitosan against pipeline steel corrosion. *J. Mol. Liq.* **2020**, *315*, 113772.
(29) Schellkes, E.; Hong, X.; Holz, M.; Huniar, U.; Ahlrichs, R.; Freyland, W. High temperature ^{93}Nb NMR and Raman spectroscopic investigation of the structure and dynamics of solid and liquid $NbCl_5$-alkali chloride solutions. *Phys. Chem. Chem. Phys.* **2003**, *5*, 5536−5543.
(30) Huglen, R.; Mamantov, G.; Smith, P.; Begun, G. M. Raman Spectral Study of NbCl, in Chloroaluminate Melts. *J. Raman Spectrosc.* **1979**, *8*, 326−330.
(31) Nakamoto, K. *Infrared and Raman Spectra of Inorganic and Coordination Compounds*; J. Wiley: New York, 4 edn. 1986.
(32) Nico, C.; Soares, M. R. N.; Rodrigues, J.; Matos, M.; Monteiro, R.; Graça, M. P. F.; Valente, M. A.; Costa, F. M.; Monteiro, T. Sintered NbO Powders for Electronic Device Applications. *J. Phys. Chem. C* **2011**, *115*, 4879−4886.
(33) Lu, H.-C.; Ghosh, S.; Katyal, N.; Henkelman, G.; Lakhanpal, V. S.; Milliron, D. J. Synthesis and Dual-Mode Electrochromism of Anisotropic Monoclinic $Nb_{12}O_{29}$ Colloidal Nanoplatelets. *ChemRxiv* **2020**, DOI: 10.26434/chemrxiv.12108612.v1.
(34) Todica, M.; Pop, C. V.; Udrescu, L.; Stefan, T. Spectroscopy of a Gamma Irradiated Poly(Acrylic Acid)-Clotrimazole System. *Chin. Phys. Lett.* **2011**, *28*, 128201−128201-4.
(35) Sánchez-Márquez, J. A.; Fuentes-Ramírez, R.; Cano-Rodríguez, I.; Gamiño-Arroyo, Z.; Rubio-Rosas, E.; Kenny, J. M.; Rescignano, N. Membrane Made of Cellulose Acetate with Polyacrylic Acid Reinforced with Carbon Nanotubes and Its Applicability for Chromium Removal. *Int. J. Polym. Sci.* **2015**, *2015*, 320631.
(36) Raba, A. M.; Bautista-Ruíz, J.; Joya, M. R. Synthesis and Structural Properties of Niobium Pentoxide Powders: A Comparative Study of the Growth Process. *Mater. Res.* **2016**, *19*, 1381−1387.
(37) Uekawa, N.; Kudo, T.; Mori, F.; Wu, Y. J.; Kakegawa, K. Low-temperature synthesis of niobium oxide nanoparticles from peroxo niobic acid sol. *J. Colloid Interface Sci.* **2003**, *264*, 378−384.
(38) Li, S.; Xu, Q.; Uchaker, E.; Cao, X.; Cao, G. Comparison of amorphous, pseudohexagonal and orthorhombic Nb_2O_5 for high-rate lithium ion insertion. *CrystEngComm* **2016**, *18*, 2532−2540.
(39) Le Viet, A.; Reddy, M. V.; Jose, R.; Chowdari, B. V. R.; Ramakrishna, S. Nanostructured Nb_2O_5 Polymorphs by Electrospinning for Rechargeable Lithium Batteries. *J. Phys. Chem. C* **2010**, *114*, 664−671.
(40) Majd, M. T.; Shahrabi, T.; Ramezanzadeh, B.; Bahlakeh, G. Development of a high-performance corrosion protective functional nano-film based on poly acrylic acid-neodymium nitrate on mild steel surface. *J. Taiwan Inst. Chem. Eng.* **2019**, *96*, 610−626.
(41) Saji, V. S. Superhydrophobic surfaces and coatings by electrochemical anodic oxidation and plasma electrolytic oxidation. *Adv. Colloid Interface Sci.* **2020**, *283*, 102245.
(42) Yilbas, B. S. Laser treatment of zirconia surface for improved surface hydrophobicity. *J. Alloys Compd.* **2015**, *625*, 208−215.
(43) Nayana, K. O.; Ranganatha, S.; Shubha, H. N.; Pandurangappa, M. Effect of sodium lauryl sulphate on microstructure, corrosion resistance and microhardness of electrodeposition of Ni−Co_3O_4 composite coatings. *Trans. Nonferrous Met. Soc. China* **2019**, *29*, 2371−2383.
(44) Shi, X.; Nguyen, T. A.; Suo, Z.; Liu, Y.; Avci, R. Effect of nanoparticles on the anticorrosion and mechanical properties of epoxy coating. *Surf. Coat. Technol.* **2009**, *204*, 237−245.
(45) Xu, Y.; Ma, S.; Fan, M.; Chen, Y.; Song, X.; Hao, J. Design and properties investigation of Ni Mo composite coating reinforced with duplex nanoparticles. *Surf. Coat. Technol.* **2019**, *363*, 51−60.
(46) Eduok, U.; Faye, O.; Tiamiyu, A.; Szpunar, J. Fabricating protective epoxy-silica/CeO2 films for steel: Correlating physical barrier properties with material content. *Mater. Des.* **2017**, *124*, 58−68.
(47) Eduok, U.; Szpunar, J. Ultrasound-assisted synthesis of zinc molybdate nanocrystals and molybdate-doped epoxy/PDMS nanocomposite coatings for Mg alloy protection. *Ultrason. Sonochem.* **2018**, *44*, 288−298.
(48) Eduok, U.; Faye, O.; Ohaeri, E.; Szpunar, J.; Akpan, I. Synthesis and characterization of protective silica reinforced hybrid poly (vinylpyrrolidone)/acrylate/silane nanocomposite coatings. *New J. Chem.* **2020**, *44*, 1117−1126.
(49) Criado, M.; Sobrados, I.; Sanz, J.; Bastidas, J. M. Steel protection using sol−gel coatings in simulated concrete pore solution contaminated with chloride. *Surf. Coat. Technol.* **2014**, *258*, 485−494.
(50) Haeria, S. Z.; Asgharia, M.; Ramezanzadeh, B. Enhancement of the mechanical properties of an epoxy composite through inclusion of graphene oxide nanosheets functionalized with silica nanoparticles through one and two steps sol-gel routes. *Prog. Org. Coat.* **2017**, *111*, 1−12.
(51) Conradi, M.; Kocijan, A.; Kek-Merl, D.; Zorko, M.; Verpoest, I. Mechanical and anticorrosion properties of nanosilica-filled epoxy-resin composite coatings. *Appl. Surf. Sci.* **2014**, *292*, 432−437.
(52) Ramezanzadeh, B.; Niroumandrad, S.; Ahmadi, A.; Mahdaviana, M.; Mohamadzadeh, M. H. Enhancement of barrier and corrosion protection performance of an epoxy coating through wet transfer of amino functionalized graphene oxide. *Corros. Sci.* **2016**, *103*, 283−304.
(53) Ammar, S.; Ramesh, K.; Ma, I. A. W.; Farah, Z.; Vengadaesvaran, B.; Ramesh, S.; Arof, A. K. Studies on SiO_2-hybrid polymeric nanocomposite coatings with superior corrosion protection and hydrophobicity. *Surf. Coat. Technol.* **2017**, *324*, 536−545.
(54) Sari, M. G.; Shamshiri, M.; Ramezanzadeh, B. Fabricating an epoxy composite coating with enhanced corrosion resistance through impregnation of functionalized graphene oxide-co-montmorillonite Nanoplatelet. *Corros. Sci.* **2017**, *129*, 38−53.
(55) Radomana, T. S.; Dzunužović, J. V.; Grgur, B. N.; Gvozdenović, M. M.; Jugović, B. Z.; Miličević, D. S.; Dzunužović, E. S. Improvement of the epoxy coating properties by incorporation of polyaniline surface treated TiO_2 nanoparticles previously modified with vitamin B6. *Prog. Org. Coat.* **2016**, *99*, 346−355.
(56) Hussein, M. S.; Fekry, A. M. Effect of Fumed Silica/Chitosan/Poly(vinylpyrrolidone) Composite Coating on the Electrochemical Corrosion Resistance of Ti−6Al−4V Alloy in Artificial Saliva Solution. *ACS Omega* **2019**, *4*, 73−78.
(57) Wen, J. G.; Geng, W.; Geng, H. Z.; Zhao, H.; Jing, L. C.; Yuan, X. T.; Tian, Y.; Wang, T.; Ning, Y. J.; Wu, L. Improvement of Corrosion Resistance of Waterborne Polyurethane Coatings by Covalent and Noncovalent Grafted Graphene Oxide Nanosheets. *ACS Omega* **2019**, *4*, 20265−20274.
(58) Taghavikish, M.; Subianto, S.; Dutta, N. K.; de Campo, L.; Mata, J. P.; Rehm, C.; Choudhury, N. R. Polymeric Ionic Liquid Nanoparticle Emulsions as a Corrosion Inhibitor in Anticorrosion Coatings. *ACS Omega* **2016**, *1*, 29−40.
(59) Quadri, T. W.; Olasunkanmi, L. O.; Fayemi, O. E.; Solomon, M. M.; Ebenso, E. E. Zinc Oxide Nanocomposites of Selected Polymers: Synthesis, Characterization, and Corrosion Inhibition Studies on Mild Steel in HCl Solution. *ACS Omega* **2017**, *2*, 8421−8437.
(60) Suleiman, R. K.; Kumar, A. M.; Rahman, M. M.; Al-Badour, F. A.; Meliani, M. H.; Saleh, T. A. Effect of metal oxide additives on the structural and barrier properties of a hybrid organosilicon sol-gel coating in 3.5% NaCl medium. *Prog. Org. Coat.* **2020**, *148*, 105825.
(61) Mazur, M.; Kalisz, M.; Wojcieszak, D.; Grobelny, M.; Mazur, P.; Kaczmarek, D.; Domaradzki, J. Determination of structural, mechanical and corrosion properties of Nb_2O_5 and $(Nb_yCu_{1-y})O_x$ thin films deposited on Ti6Al4V alloy substrates for dental implant applications. *Mater. Sci. Eng., C.* **2015**, *47*, 211−221.
(62) Dinu, M.; Braic, L.; Padmanabhan, S. C.; Morris, M. A.; Titorencu, I.; Pruna, V.; Parau, A.; Romanchikova, N.; Petrik, L. F.; Vladescu, A. Characterization of electron beam deposited Nb_2O_5 coatings for biomedical applications. *J. Mech. Behav. Biomed. Mater.* **2020**, *103*, 103582.

https://dx.doi.org/10.1021/acsomega.0c04948
ACS Omega 2020, 5, 30716−30728